Density and Pressure Fluctuations in Gas Fluidized Beds

OLAF WINTER

The Goodyear Tire & Rubber Company, Akron, Ohio

A Bench-scale size fluidization system was constructed for the purpose of conducting experiments to determine density and pressure fluctuations in gas fluidized beds. Density fluctuations and bubble sizes were measured with a photocell device and β-ray absorption. Pressure fluctuations were determined with a conductivity cell. The frequency distributions of the density and pressure fluctuations and bubble sizes were determined as functions of several variables. They could be described by dimensionless coefficients and χ^2-distributions with different degrees of freedom. Such variables as distance from the gas distribution plate, bed height, particle size, gas flow rate, and internal screens were considered.

The characteristics of fluidized beds are a complex function of particle characteristics, bed geometry, and properties and flow conditions of the fluid.

One of the characteristics of gas fluidized beds is the density of the system. An average density can be calculated from the bed volume and solid weight. The true density however, is in an unsteady state and not locally constant. This means that a gas fluidized bed is characterized by the presence of density fluctuations, caused by bubbles, which form spontaneously and grow in size as they rise through the bed. This action is an important factor in the performance of the bed in terms of mass transfer, heat transfer, or chemical reaction accomplished. Therefore, it is important and interesting to characterize density behavior at different conditions.

Several investigators examined fluid-bed densities and their relation to system conditions by various experimental techniques. Measurements of density fluctuations have also been carried out indirectly through measuring of pressure fluctuations of the fluid, caused by rising bubbles. However, the functional relation between pressure and density fluctuations and their distributions have not yet been described quantitatively.

The purpose of this paper is to define characteristic numbers for density and pressure fluctuations for gas fluidized beds by means of these experiments, and discuss their functional relationship and relation to several reaction conditions based on a statistical treatment of locally observed data.

These quantitatively described properties lead to a better understanding of fluidized bed behavior and hence will improve scaling-up of data and design of equipment.

EXPERIMENTAL PROCEDURE

The arrangement of equipment is indicated schematically in Figure 1 and described in detail elsewhere (*3, 8, 9, 13*). The experiments were carried out in a vertical cylindrical glass column with 5.3 in. I.D. The column was flanged at top and bottom to provide for a solid support grid and for necessary taps for sampling, measuring, and filling. The support grid was a 1/16 in. porous stainless steel plate with a pore size of 35μ.

Local density fluctuations were measured with a photocell probe. The method is based upon the transmission of light between small probes submerged within the fluidized bed and conversion of the light signal to electrical impulses which are amplified and recorded. The sensing element of the probe consisted of a 2 × 6 mm. 4 volt light source coupled with a 2 × 6 × 8 mm. Germanium photodiode (Siemens, TP 50) with a sensitive area of 1 sq. mm. The light source and detector were separated by fixed distances of 2 or 13 mm.

Some local density fluctuations were measured with a strontium 90 β-ray source of 25 mC which were located in a 2 × 15 mm. Monel tube and surrounded by an aluminum cover of 0.1 mm. wall thickness. Instruments for detecting the transmitted radiation and for indicating and recording the resulting signal were chosen for their rapid response to changes in the level of the transmitted radiation. The radiation was sensed by a 7 × 70 mm. Geiger-Mueller detector, the electrical pulses amplified and recorded on a high speed oscillograph (Hellige He/b). The distance between radiation source and detector was 2.5 mm.

Pressure fluctuations were transmitted from the fluidized bed through a 7 mm. I.D. glass tube to a conductivity cell. A change in pressure caused a change of a liquid level in the

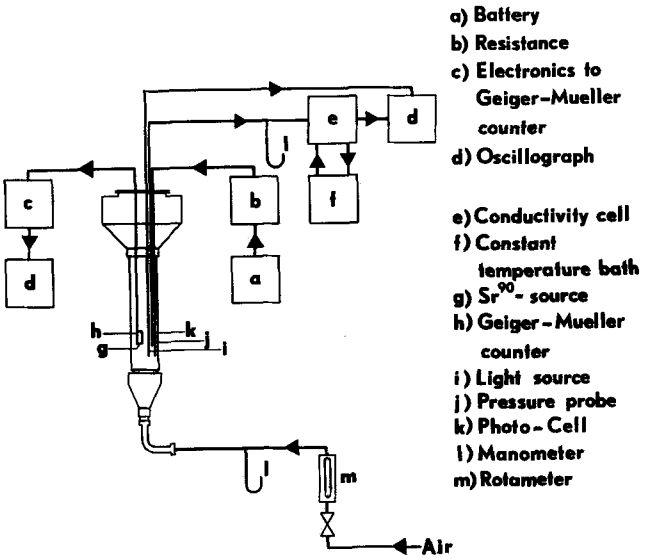

Fig. 1. Arrangement of experimental equipment.

cell, which directly affected the resistance of a platinum electrode. The resulting electrical signal was amplified and recorded. The conductivity cell was coupled with a reference cell in a Wheastone bridge arrangement. The actual pressure was measured with an U-shape mercury manometer and the mean of twenty readings per sample point used. The response of the conductivity cell was tested. Recorded amplitudes of pressure fluctuations between 2 and 8 cycles/sec. were practically independent from the frequency. Almost all of the recorded pressure fluctuations were in this range.

The photocell probe was coupled with the pressure probe and both, pressure and density fluctuations, were simultaneously detected and recorded by means of a high speed oscillograph. The frequency range of Philips' 4 channel Oscilloscript (platinum 1,000/4) was 0 to 165 cycles/sec. All measurements were made in the radial center of the bed with the exception of a run series, designed to investigate the detecting capability of the equipment (Figure 9).

All tubes which were introduced into the fluidized bed were equipped with micrometallic filter tips.

Air from a central laboratory compressor was reduced in pressure, filtered, and metered through rotameters. The solids used were glass beads with uniform particle diameters and a density of 2.88 g./cc. Under the microscope the glass beads appeared almost spherical.

Some experiments were carried out with horizontal screen inserts made from galvanized wire hardware cloth of 10, 13, 16, 20, 24, 26, and 28 mesh.

EVALUATION OF DENSITY AND PRESSURE FLUCTUATIONS

Fluidized beds are in a quasi stationary state. This means that the mean values of their physical properties are time independent over a finite period of time.

Local density and pressure fluctuations obey probability laws. Therefore, they can be evaluated by means of statistical analysis.

Pressure fluctuations have been graphically recorded for six seconds at each sample point. They were evaluated by counting the number of crossings of the curve with each horizontal line of a millimeter scale. This determined the frequency of a certain pressure value belonging to a certain millimeter line for a time of six seconds. The average number of observations were between sixty and one hundred twenty, or about one observation for every 1/15th of a second. The cummulative frequencies of these distributions were plotted on normal probability paper and the first (R_1), second (R_2), and third (R_3) quartiles determined graphically for each curve.

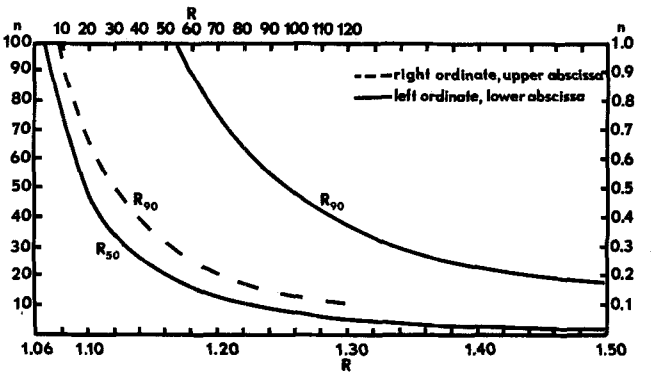

Fig. 2. Diagram for the determination of the degree of freedom for χ^2-distribution and Γ-functions.

The most probable deviation from the mean value, the interquartile or T_{50} -- range, Q_3 minus Q_1, which gives the length of the interval containing the middle 50% of observations, was multiplied by 100 and divided by the actual measured gas pressure. The resulting value v_{50} represents the relative intensity of the pressure fluctuations.

The assymmetry of distributions can be described by degrees of freedom. Therefore, the frequency distribution of the pressure fluctuation may be characterized by such a value n_{50}, provided that the distributions can be approximated with a χ^2-distribution or a Γ-function (*1*). It could be shown that this was almost always the case.

The characteristic value for asymmetry, R_{50}, was calculated from $R_{50} = (Q_3 - Q_2)/(Q_2 - Q_1)$. R_{50} values have also been calculated for different degrees of freedom, n_{50}, for χ^2-distributions and Γ-functions, utilizing tables of Bennet and Franklin (*1*), and Pearson (*2*). This is graphically represented in Figure 2. By the use of this figure one can determine n_{50} directly for any value of R_{50}, calculated from experimental data which were graphically evaluated.

In cases, when $R_{50} < 1$, the ratio $1/R_{50} = (Q_2 - Q_1)/(Q_3 - Q_2)$ has been used for the determination of n_{50}, it is because χ^2-distributions can describe distributions with positive skewness only. In these cases the distributions were considered to be the mirror images to the (χ^2) axis and were provided with a negative sign. The negative sign is only a connotation that the asymmetry corresponds to a negative skewness (Figure 3).

The numeral subscripts of n and R indicate that the

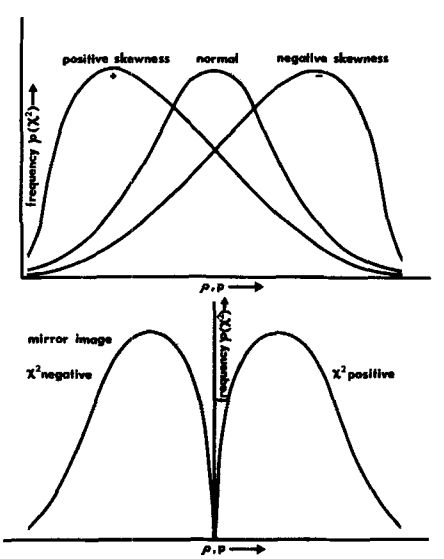

Fig. 3. Explanation of the character of frequency distributions.

middle 50% of observations were considered for determining the asymmetry of the distributions.

The density fluctuation curves, obtained through β-ray and light absorption were evaluated in a similar manner. Here, the peaks of the radiation or light intensities, that are the maxima of the recorded curves have been counted for twelve seconds and ordered in the sequence of peak heights. A longer recording time was required here for a meaningful statistical evaluation of data, because less observations were made per time unit compared to the recorded pressure fluctuations. This is due to the nature of the measuring equipment and will be discussed later.

The light or radiation absorption depends on the product of density and thickness of the material between ray source and sensor. The product is defined as area weight and has the dimensions of a weight divided by the square of a length. The recorded peak heights of light or radiation absorption were converted into area weights with the help of calibration curves, which were obtained as follows: A bulk density, calculated from the bulk volume and its weight, was multiplied by the thickness of the bulk material between ray source and sensor. This thickness was changed stepwise by putting pieces of material with known density, thickness, and absorption capability into the bulk material. Glass pieces were used for light and aluminum for radiation absorption. The area weights were determined for each particle size of bulked glass beads and plotted against the corresponding recorder amplitude.

The following simplification was made for converting area weights into bubble sizes. It was assumed that only a part of the sample volume is filled with a fluid—solid mixture of a density equal to the average density of the entire bed. The remaining part is assumed to be entirely free of solids. This corresponds to a solid free bubble. The mean area weight was divided by the mean density of the bed, and a value was obtained with the dimension of a length. The difference between the ray source and sensor and this length is defined as the diameter, d_{Bl}, of the bubble.

The frequency distributions of the peak heights were converted into bubble size distributions. The mean bubble size d_{Bl} was calculated as a weighted arithmetic mean of all peak heights. These mean values correspond to mean area weights of the calibration curves. The variations of the bubble sizes were determined graphically by plotting the cumulative frequency distributions on normal probability paper and determining the fifth (P_5), ninety-fifth percentile (P_{95}), and the second quartile for each sample point. The 90% interpercentile or T_{90} — range, which gives the length of the interval containing the middle 90% of observations, was designated as the variation of the bubble size. The value v_{90}, calculated from the ratio $v_{90} = T_{90}/\bar{d}_{Bl}$ is the relative variation of the frequency distribution. The T_{90} — range has been used in favor of a smaller range, because of the high degree of skewness of the density frequency distributions. The T_{50} — range, for example, would have resulted in large errors.

The character of the bubble size frequency distributions were determined graphically from $R_{90} = (P_{95} - Q_2)/(Q_2 - P_5)$, and expressed in degrees of freedom, n_{90}. The precalculated curves (Figure 2) for the relation of R_{90} to n_{90} for χ^2-distributions were used for the direct determination of n_{90}. P_5, Q_2, and P_{95} are area weights corresponding to 5, 50, and 95% of the cumulative distribution.

χ^2-distributions do not have degrees of freedom smaller than one. Therefore, degrees of freedom smaller than one cannot be approximated with χ^2-distributions. In such cases the χ^2-distribution has been extended with a Γ-function, and n_{90} was calculated on the basis of the relation between q_{90} and n_{90} by using the equation $q + 1 = n/2$. On the basis of the asymmetry of the Γ-function, q_{90} can be determined with R_{90} in a similar manner with n_{90}. The corresponding summation function of these distributions are:

$$\phi(\chi^2, n) = \frac{\left(\frac{\chi^2}{2}\right)\int_0^\infty e^{-x^2/2}\left(\frac{\chi^2}{2}\right)^{(n/2)-1} d\left(\frac{\chi^2}{2}\right)}{\int_0^\infty e^{-x^2/2}\left(\frac{\chi^2}{2}\right)^{(n/2)-1} d\left(\frac{\chi^2}{2}\right)}$$

$$= \frac{1}{\left(\frac{n}{2}-1\right)!}\int_{\left(\frac{\chi^2}{2}\right)}^\infty e^{-x^2/2}\left(\frac{\chi^2}{2}\right)^{(n/2)-1} d\left(\frac{\chi^2}{2}\right)$$

$$\phi(\chi, q) = \frac{\int_X^\infty e^{-x} X\, q\, dx}{\int_0^\infty e^{-x} X\, q\, dx} = \frac{1}{\Gamma(q+1)}\int_X^\infty e^{-x} X\, q\, dX$$

$$\frac{\chi^2}{2} = X \qquad \frac{n}{2} - 1 = q$$

$$q! = \Gamma(q+1)$$

The numeral subscripts of q, n, and R indicate that the middle 90% of observations were considered for determining the asymmetry of the distributions.

The distributions have been recorded in such a manner that the density or the pressure increases in the positive direction of the abscissa (Figure 3). All positive n values have higher frequencies of smaller densities or smaller pressures than the normal distribution. Negative n values have higher frequencies of larger densities or pressures than the normal distribution. If n goes to infinity, the distributions from both directions approximate symmetric normal distributions.

FREQUENCY DISTRIBUTIONS OF BUBBLE SIZES

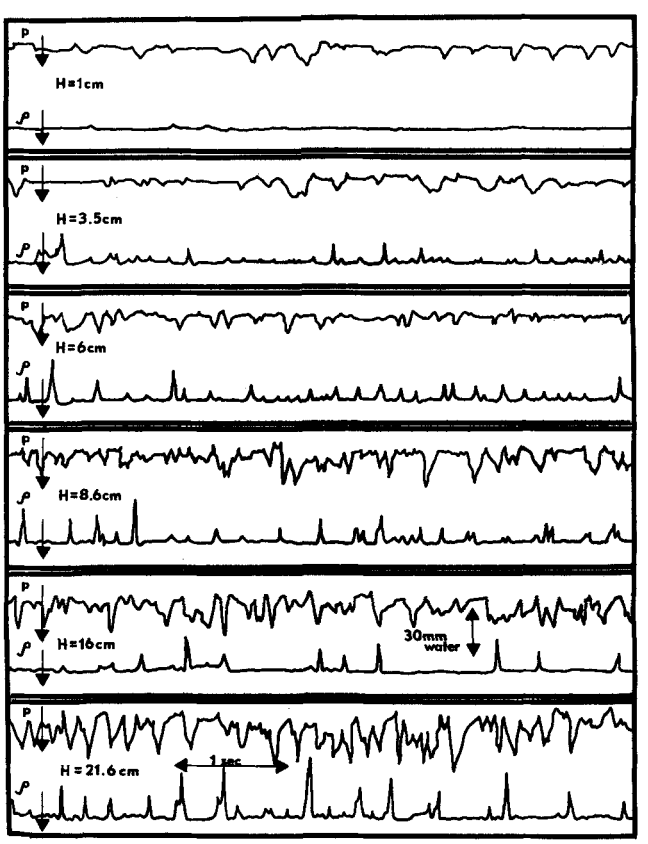

Fig. 4. Local density and pressure fluctuations at different distances from the distribution plate for 110μ glass beads. V = 0.488 SCFM.

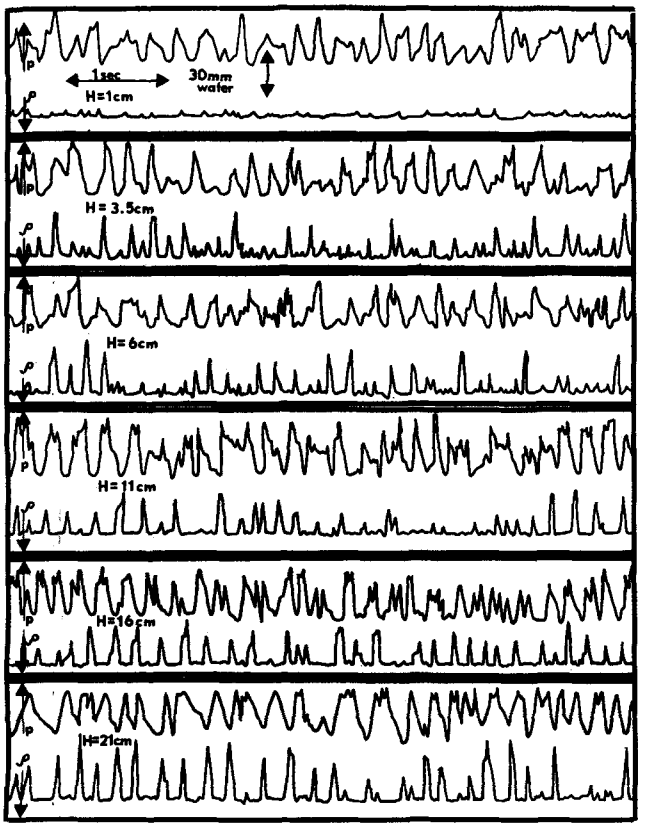

Fig. 5. Local density and pressure fluctuations at different distances from the distribution plate for 250μ beads. V = 4.229 SCFM.

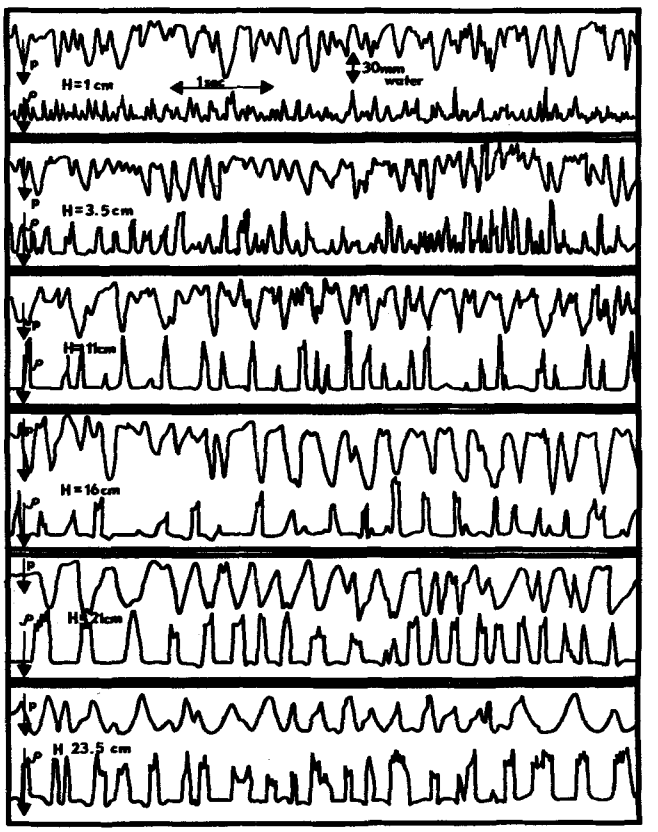

Fig. 6. Local density and pressure fluctuations at different distances from the distribution plate for 500μ glass beads. V = 11.421 SCFM.

Properties of bubbles in gas fluidized beds have been investigated by various techniques. Such properties as the rate of rise, average and maximum size, coalescence, stability and other characteristics of bubbles have been described by a number of investigators. A survey of late publications on these subjects can be found elsewhere (*4*). However, the distribution of bubble sizes within a gas fluidized bed has not yet been described in detail.

In this work, locally measured density fluctuations were used to determine bubble size distributions. Figures 4, 5, and 6 show examples of curves or recorded density and pressure fluctuations which were recorded simultaneously and evaluated statistically. The arrows indicate in which direction the higher values for pressure or density are recorded. Changes of the local solid concentration caused by bubbles are shown as wedge shaped peaks. The size of the bubble is indicated by the height and the duration of the peak. The height of the peak depends on the horizontal diameter and the duration on the vertical diameter of the bubble. The latter is of less value because of its ill defined lower boundary, due to the presence of a diluted bulk of solid, carried upwards by the bubble in its wake. In Figure 4, curves are shown for a bed with fluidized uniform glass beads of 110μ. The frequency of the bubbles increases with the distance from the distribution plate H to about the middle of the bed and decreases from there on. The size of the bubbles definitely increases with H. A similar pattern can be recognized in beds with 250μ and 500μ glass beads (Figures 5 and 6). The frequencies, however, decrease all the way with increasing H in beds with 250μ and 500μ beads, while the light absorption increases in beds of 500μ to H = 11 cm. only and then remains constant. An increase in the width of the absorption peaks indicates that the actual size of the bubbles increases further with H. However, the heights of the peaks are not affected further because the bubble diameters exceed the distance between light source and photocell.

Some results of the statistical evaluation of curves are shown in Table 1. In Figure 7 some cumulative distributions of bubbles are plotted on probability paper.

The mean bubble diameter, $\bar{d}_{Bi}$, increases with the distance from the distribution plate, H, because of coalescence and decrease of effective hydrostatic pressure acting on the bubbles. The mean bubble diameter increases also with the gas velocity V. This confirms the results of a number of investigators, which have approached these problems with other experimental techniques (5 to 7).

In general, the relative density fluctuation v_{90} follows

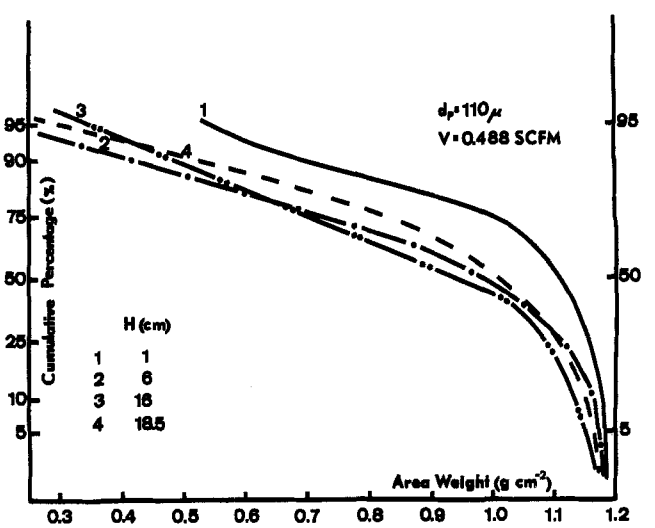

Fig. 7. Cumulative frequency distribution of bubble sizes.

Table 1. Dependency of the Mean Bubble Diameter, $\overline{d}_{Bl}$, the Relative Intensity of Density Fluctuations, v_{90}, and the Degree of Freedom of the Bubble Size Frequency Distribution, n_{90}, on the Distance from the Distribution Plate, H, and the Gas Velocity, V (N = normal distribution)

	Std. cu. ft./ min.	H, cm.	1.0	3.5	6.0	8.5	11.0	13.5	16.0	18.5	21.0	23.5	26.0
$d_p = 110\mu$	0.488	$\overline{d}_{B1}$	—	6.2	7.3	7.4	8.5	7.6	7.3	9.6	10.7	10.0	8.6
$L_o = 26$		v_{90}	0.0	0.62	0.78	1.17	1.21	1.07	1.05	2.23	3.20	2.27	1.85
cm.		n_{90}		−1	−2	−2	−2	−2	−2	−8	−8	−2	−2
	0.598	$\overline{d}_{B1}$	5.4	5.7	6.8	7.9	8.1	8.4	7.8	9.3	10.0	9.2	8.6
		v_{90}	0.0	0.29	1.18	1.47	1.42	1.58	1.44	2.58	2.67	2.11	1.68
		n_{90}		−2	−0.8	−1	−2	−9	−1	−3	−5	−5	−2
	0.734	$\overline{d}_{B1}$	7.1	8.3	8.3	9.0	8.0	9.4	9.0	10.7	11.0	9.7	10.5
		v_{90}	0.99	1.66	1.66	1.95	1.01	2.20	2.02	3.59	3.98	5.00	3.18
		n_{90}	−0.9	−3	−3	−7	−1	−5	N	−46	N	−31	N
$d_p = 250\mu$	2.986	$\overline{d}_{B1}$	0.4	0.4	0.4	0.4	0.4	4.9	4.9	4.6	6.6	5.2	
$L_o = 22$		v_{90}	0.0	0.0	0.0	0.0	0.0	1.19	1.50	0.99	1.85	1.14	
cm.		n_{90}						−3	−2	−2	−36	N	
	3.446	$\overline{d}_{B1}$	0.4	3.9	5.0	5.0	5.2	6.3	7.9	8.0	8.4	8.9	
		v_{90}	0.0	0.75	1.05	1.02	1.25	1.72	2.50	2.54	2.56	2.91	
		n_{90}		−4	−15	N	−2	N	−11	N	+4	+3	
	3.858	$\overline{d}_{B1}$	0.4	4.9	6.6	5.4	5.9	6.2	7.6	7.2	7.9	7.9	
		v_{90}	0.0	1.14	1.54	1.15	1.14	1.45	2.20	2.02	2.51	3.19	
		n_{90}		−5	N	N	N	N	N	N	N	+4	
	4.229	$\overline{d}_{B1}$	1.0	5.5	6.1	6.1	7.2	7.1	8.1	8.3	9.9	10.0	
		v_{90}	0.20	1.28	1.45	1.55	1.83	1.81	2.32	2.36	3.50	3.40	
		n_{90}		−35	−25	N	+20	+20	+5	+10	+4	+2	
$d_p = 500\mu$	10.508	$\overline{d}_{B1}$	1.3	5.2	6.6	6.9	9.0	10.9		>12.0	>12.8	>12.9	
$L_o = 21.5$		v_{90}	0.0	1.00	1.66	1.92	2.84	5.37		11.0	60.33	50.67	
cm.		n_{90}		−6	−8	−4	−18	N		N	+0.2	+0.1	
	11.421	$\overline{d}_{B1}$	3.7	7.0	7.7	8.3	8.8	10.7	11.5	>12.2	>12.6	>12.9	
		v_{90}	0.82	1.80	2.07	2.4	2.70	5.06	6.44	14.3	29.5	51.3	
		n_{90}	N	−9	N	N	N	+2	+1	+2	+1	+1	

the same trend. The character of the bubble size frequency distribution is not uniform. Small particle sizes and low gas velocities have small negative n_{90} values, which remain rather constant in the entire bed. With larger gas velocities, n_{90} increases with H to infinity, which means that in these cases n_{90} can be approximated with a normal distribution. The same tendency can be observed with 250μ particles and low gas velocities. At a medium gas velocity the normal distribution is reached rapidly and remains constant over a wide range. At high gas velocities, n_{90} has negative values just above the distribution plate, and approaches normal distributions with increasing H until positive values are reached in the upper part of the bed. With small particle sizes and at low gas velocities the small bubbles affect the frequency distributions in such a manner that the frequency of the bubbles decreases exponentially with increasing bubble diameter. At $n_{90} = 2$ the exponential relation is perfectly valid, because the χ^2 distribution is simplified to

$$\phi(\chi^2) = \frac{1}{2} e^{-\frac{\chi^2}{2}}$$

where the bubble diameter is represented by χ^2. This relation is only approximated for other small values of n_{90}.

If n approaches infinity, the χ^2 distribution turns into a normal distribution

$$\phi(\chi^2) = \frac{1}{\sigma\sqrt{2\pi}} e^{-(x-\mu)^2/2\delta^2}$$

where the variance of the distribution is $\sigma^2 = \frac{1}{2}$ and the mean is $\mu = \sqrt{n-1}$. Therefore, the value of $\sqrt{2\chi^2} - \sqrt{2n-2}$, which represents the bubble diameter, is normally distributed with a variance $\sigma^2 = 1$ and a mean $\mu = 0$. With these distributions the mean bubble size is most frequent, and the frequency decreases with increasing distance of the mean bubble size.

For medium particle sizes and at medium gas velocities the bubble size distributions are often approximated by a normal distribution. With large particle sizes and at high gas velocities, large bubbles are rather frequent. In some cases, especially at greater distances from the distribution plate, the distributions are strongly asymmetric. At a specific value the frequency of the bubble size decreases almost exponentially with the bubble diameter.

PRESSURE FLUCTUATIONS

A number of papers have been published in which pressure fluctuations were used to determine the inhomogeneity of fluidized beds (*8* to *11*). However, the relationship between the intensity of pressure fluctuations and the intensity of density fluctuations has not yet been investigated.

In order to determine this, artificial bubbles were injected into a fluidized bed of 50μ glass beads with a piston machine, driven by a synchronous motor. The fluidized bed appeared to be perfectly homogeneous at low gas velocities. Injection tubes of 1.5 mm. I.D. were used. The equal volume of the bubbles and the time interval between injections was controlled by a mechanical gear device on the motor. The light absorption and pressure fluctuations were measured simultaneously as before. However, the distance between the light source and photocell was reduced to 2 mm. and a metal tube of only 2 mm. O.D. was used for transmission of pressure fluctuations to the conductivity cell.

Figure 8 shows pressure waves produced by the piston machine in the fixed bed without gas flow (*a*), with gas flow (*b*), with gas velocity at the fluidization point (*c, d*), and in the fluidized bed (*e, f*).

The pressure waves produced bubbles in the fluidized bed, which appeared as acute maxima of the light intensity curves (e, f). If the sample was taken above the bubble source in a radial distance $x = 0$, the pressure maxima (p) and the minima of the solid concentration coincided (Figure 9). If the sample tube was moved in a radial direction, the minima of the solid concentration disappeared slowly with the distance x from the bubble source. The pressure fluctuations remained, but they became more and more dampened with increased distance from the bubble path. Further investigations indicated

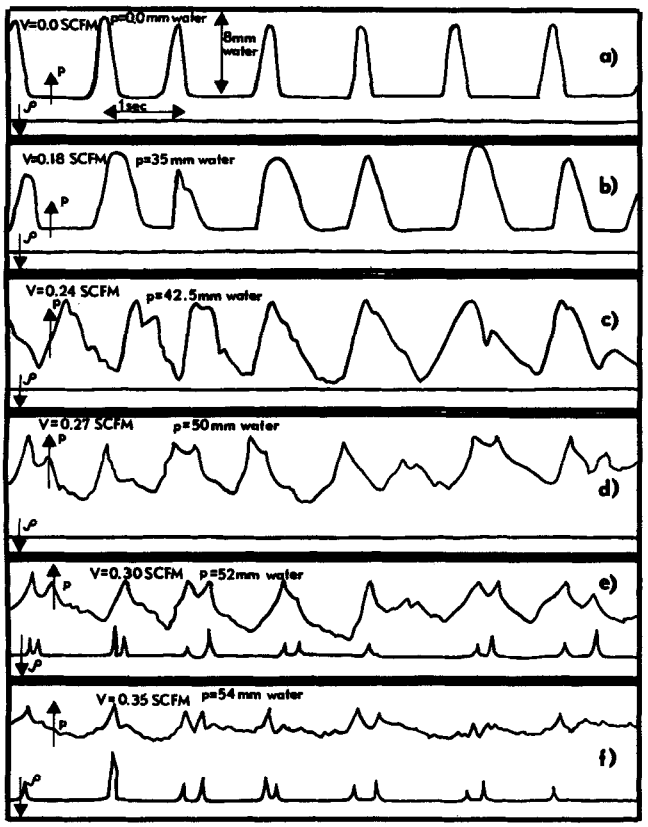

Fig. 8. Local density and pressure fluctuations in a homogeneous bed of 50μ glass beads with artificially injected bubbles.

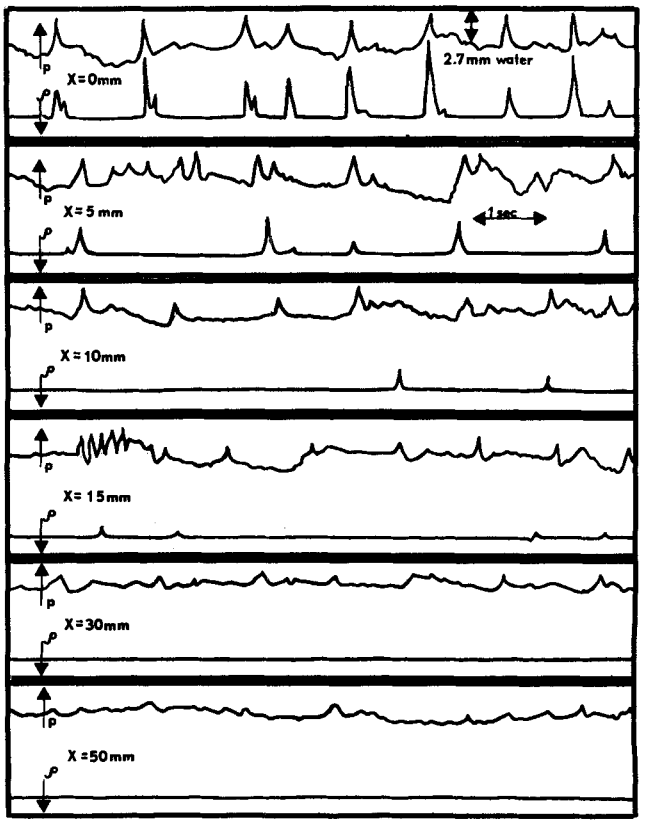

Fig. 9. Dependency of local density and pressure fluctuations on the distance from artificially injected bubbles. $d_p = 50\mu$, $V = 0.336$ SCFM.

that the pressure probe does not record bubbles if the bubble source is above the sample point.

The rising bubble produced a pressure wave, whose intensity decreased as the distance from the bubble path increased. A pressure probe in a fluidized bed recorded all bubbles undamped, which hit the probe directly. In addition, all bypassing bubbles were recorded. But the greater the distance of the bubble from the probe, the more damped was the recording of its pressure wave. If the pressure fluctuations are always measured at the same point of a cross section, the inhomogeneity can be characterized for this specific cross section, provided that the

TABLE 2. DEPENDENCY OF THE RELATIVE INTENSITY, v_{50}, AND THE CHARACTER n_{50}, OF THE PRESSURE FLUCTUATIONS ON THE DISTANCE FROM THE DISTRIBUTION PLATE, H, AND THE GAS VELOCITY, V (N = NORMAL DISTRIBUTION)

	Std. cu. ft./ min.	H, cm.	1.0	3.5	6.0	8.5	11.0	13.5	16.0	18.5	21.0	23.5	26.0
$d_p = 110\mu$	0.488	v_{50}	0.1	0.1	0.2	1.3	2.4	4.6	6.4	8.5	14.4	26.0	43.0
$L_o = 26$ cm.		n_{50}					+2	+4	+6	+45	N	N	
	0.598	v_{50}	2.2	1.5	1.1	1.4	3.3	4.9	7.9	13.8	18.3	36.0	80.0
		n_{50}	+1	+1	+1	+1	+1	+4	+2	+11	+6	+12	−27
	0.734	v_{50}	2.5	2.3	2.2	3.6	5.1	7.8	9.7	12.3	22.8	42.0	113.3
		n_{50}	+3	+2	+27	+3	+32	+2	+2	+4	+8	N	−9
$d_p = 250\mu$	2.986	v_{50}	0.0	0.0	0.0	0.0	0.0	2.3	2.6	8.7	27.1	60.0	
		n_{50}						+2	+6	+1	+1	+50	
$L_o = 22$ cm.	3.446	v_{50}	0.7	0.8	3.5	1.5	2.6	5.8	12.2	20.0	44.3	110.0	
		n_{50}	−11		+6	N	+9	+1	+37	N	N	N	
	3.858	v_{50}	1.9	1.9	3.3	4.5	6.2	9.0	14.3	13.3	37.1	140.0	
		n_{50}	N	N	+3	+3	+4	+7	−27	+33	+24	−8	
	9.229	v_{50}	2.6	4.9	5.6	6.6	7.7	10.6	14.3	20.7	47.1	240.0	
		n_{50}	+7	+14	+1	+9	+9	N	−27	−12	N	−5	
$d_p = 500\mu$	10.508	v_{50}	0.7	1.0	3.8	5.3	7.6	13.1	21.3	41.5	61.4	50.0	
		n_{50}	+6	+2	+3	+3	+3	+4	+6	+7	N		
$L_o = 21.5$ cm.	11.427	v_{50}	3.9	4.4	4.5	7.3	7.6	12.1	19.0	40.8	72.9	200.0	
		n_{50}	N	N	N	N	N	N	+13	+7	+24		

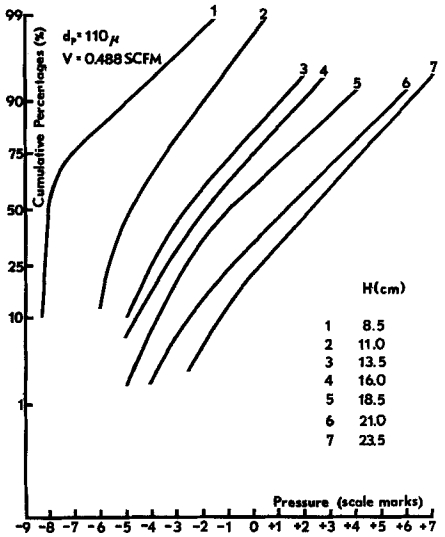

Fig. 10. Cumulative frequency distribution of local pressure fluctuations.

bubble distribution is the same for this level. This method can be used to obtain a useful weighted mean value or a characteristic frequency distribution for any cross section.

Figures 4, 5, and 6 show that an expected direct relation between individual pressure maxima (p) and density maxima (ρ) cannot be proved. The above described model experiment has given the explanation for that. However, certain general ralations between pressure and density fluctuations can be observed.

The amplitude of the pressure fluctuations increases with H similar to the density fluctuations.

The statistical evaluation of the data results in a more accurate description of the pressure fluctuations.

Figure 10 shows some cumulative distributions of pressure fluctuations on probability paper. They indicate that the character and the width of the probability distributions depend on H. The abscissa shows the pressure fluctuations as recorded in scale marks of the recording system. Negative values indicate a pressure lower and positive values a pressure higher than the actual pressure. A calibration curve was used for the conversion from scale marks to actual pressure.

Table 2 shows statistically evaluated values of pressure fluctuations of some of the investigated fluidized beds. The relative intensity of the pressure fluctuations, v_{50}, increases definitely with the distance of the distribution plate H and the gas velocity V. Larger particle sizes require greater gas velocities in order to achieve a comparable fluidization state, and are therefore, generally characterized by a greater relative intensity of pressure fluctuations.

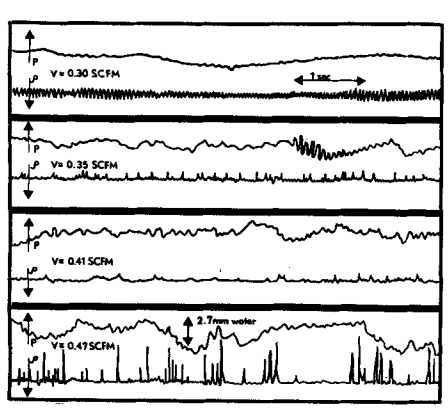

Fig. 11. The effect of gas velocity on the local density and pressure fluctuations near the fluidization point. $d_p = 50\mu$.

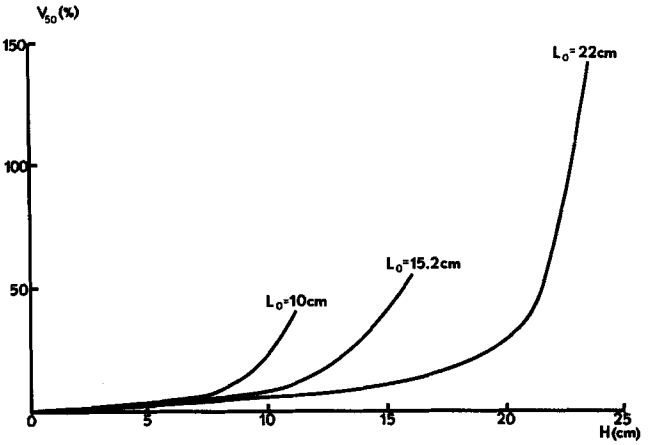

Fig. 12. Dependency of relative intensity of pressure fluctuations, V_{50}, on the bed height.

The degree of freedom of the distributions, n_{50}, moves with increasing H from small positive values to infinity (normal distribution), and further to small negative values. This has been expected, because the frequency distributions of density and pressure fluctuations behave somewhat like mirror images for reasons mentioned above. High densities (small bubbles) and small pressure maxima are more frequent in fluidized beds of small particles than those with low density and large pressure maxima. Low densities (large bubbles) and large pressure maxima dominate the frequency distributions in beds of large particles.

The simultaneous measurement of density and pressure fluctuations made it also possible to investigate the process of particle movement of the bed at the fluidization point. In a bed of 50μ glass beads no pressure fluctuations (p) could be observed at low gas velocities, although the photocell device already recorded density fluctuations (ρ) with a high frequency of about 30 cycles/sec. (Figure 11). These fluctuations could only be produced by quasi-oscillation of the particles. This confirms the theory of Baerns (*12*) that the kinetic energy of fluidized particles consists of translation, rotation, and oscillation energy. With increasing gas velocity, these density fluctuations disappear slowly, while the pressure probe already indicates some pressure fluctuations. At V = 0.41 std. cu. ft./min. the bed is perfectly homogeneous. At further increases of V, bubbles are produced and appear as acute peaks on the recorder. Besides the short term pressure fluctuations, longer term changes also can be observed. These changes indicate that a stationary state does not exist at a certain range of gas velocities in which the bed collapses and expands alternately. In this range, the appearance of bubbles as well as longer term pressure fluctuations are periodic. This can be seen in Figure 11. With larger particles, the process of particle movement develops in a similar manner. However, the unstable range is shorter and the bed collapses less often at a specific gas velocity range close to the fluidization point.

The v_{50} values increase strongly with decreasing bed height, if they are compared at the same height level. A comparison of three beds with the same size of particles is shown in Figure 12.

THE EFFECT OF SCREENS ON THE PRESSURE AND DENSITY FLUCTUATIONS

The effect of screens on pressure and density fluctua-

tions and bubble sizes is obvious. Some data are shown in Figures 13 and 14. Further results can be found elsewhere (*13*, *14*). The screens diminish the pressure and density fluctuations and reduce the mean bubble size. One screen has only a small influence, but two or more screens show a stronger effect. The number of screens affect the mean of the pressure fluctuation intensity, v_{50}, more than the number of meshes per sq. cm. (Figure 13). However, in general v_{50} decreases a few percent with each increase in the number of meshes/sq. cm. screen area.

The trends of the pressure, density fluctuations, and bubble sizes relative to the distance from the distribution plate, the gas velocity, particle size, and bed height, remain the same after screens are inserted into a fluidized bed.

The effect of the number of meshes per sq. cm. on v_{90} and d_{Bl} is strong. The more meshes per sq. cm. screen area

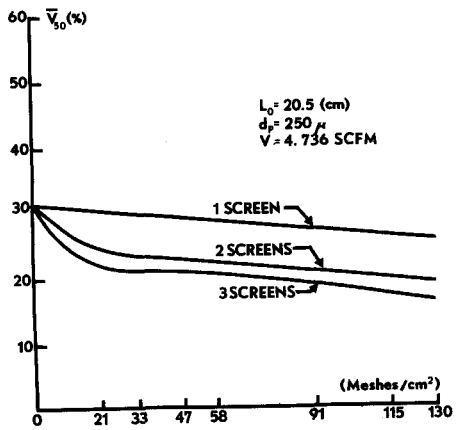

Fig. 13. Dependency of the average relative intensity of pressure fluctuation on the number of screens and number of meshes per sq. cm. screen area.

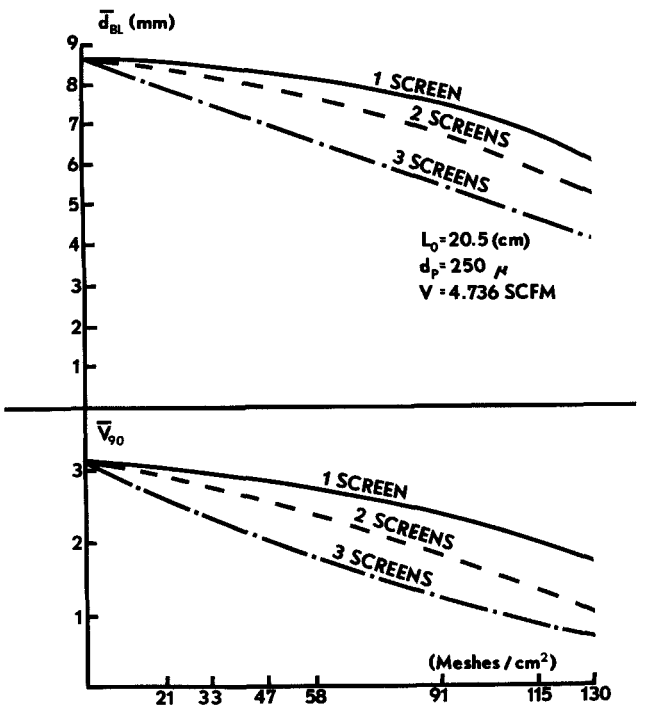

Fig. 14. Dependency of the average bubble diameter and the average relative intensity of density fluctuation on the number of screens and number of meshes per sq. cm. screen area.

the lower the v_{90} values, and the smaller the bubble diameters (Figure 14). Only at high gas velocities, above a certain point, the number of meshes seem to be no longer effective.

CONCLUSIONS

By means of these experiments and application of statistical evaluation methods, characteristic numbers were defined for local density, pressure fluctuations, and bubble sizes, and their frequency distributions in fluidized beds.

The mean bubble size, and the intensity of density fluctuations definitely increase with the distance from the distribution plate H, and the gas velocity V. This confirms the results of a number of investigators who have approached these problems with other experimental techniques.

Small particles and low gas velocities have strongly asymmetric density distributions. Larger densities (small bubbles) are more frequent than small ones. The frequency of the bubbles decreases exponentially with increasing bubble sizes.

At larger gas velocities the density and bubble distributions are often approximated by normal distributions.

Larger particles and high gas velocities also have strongly asymmetric density distributions. However, the small densities (large bubbles), are more frequent here than large ones. In extreme cases the bubble frequency increases exponentially to a certain limit with increasing bubble size.

The character of the pressure fluctuation intensity was similar to those of the density fluctuations. The dependency of V and H was the same. The frequency distributions of the pressure fluctuations are a mirror image of the density fluctuations. This was proved with artificially injected bubbles. Artificial bubbles also showed the presence of particle oscillation. This confirms the theory that the kinetic energy of fluidized particles consists of translation, rotation, and oscillation energy.

Screen inserts diminish the pressure and density fluctuations and reduce the mean bubble size. These effects become pronounced as the number and the fineness of the screens are increased. However, at high gas velocities above a certain point, the increase in the number of meshes/sq. cm. screen area are no longer effective.

NOTATION

d_{Bl} = bubble diameter, mm.
$\bar{d}_{Bl}$ = mean bubble diameter, mm.
d_p = particle diameter
H = distance from the distribution plate, cm.
L_o = bed height at fluidization point, cm.
N = normal distribution, (—)
n_{50} = degree of freedom of χ^2-distribution, calculated from R_{50}, (—)
n_{90} = degree of freedom of χ^2-distribution, calculated from R_{90}, (—)
p = gas pressure, mm. water
P_5, P_{95} = percentile 5, 95, g./sq. cm.
q = degree of freedom of Γ-function, (—)
Q_1, Q_2, Q_3 = 1, 2, and 3 quartile, mm. water
R_{50} = characteristic number of asymmetry, calculated from Q_1, Q_2, and Q_3, (—)
R_{90} = characteristic number of asymmetry, calculated from P_5, P_{95}, and Q_2, (—)
T_{50} = most probable deviation from the mean of pressure fluctuations, calculated from Q_3 and Q_1, mm. water
T_{90} = deviation from the mean of density fluctuations, calculated from $P_{95} - P_5$, g./sq. cm.

V = volumetric gas velocity, std. cu. ft./min.
v_{50} = relative intensity of pressure fluctuations, %
$\bar{v}_{50}$ = mean relative intensity of pressure fluctuation, %
v_{90} = relative intensity of density fluctuations, (—)
$\bar{v}_{90}$ = mean relative intensity of density fluctuation, (—)
x = distance from bubble, mm.

Greek Letters

μ = mean of distribution
ρ = density, g./cc.
σ^2 = variance of distribution
$\phi(\Gamma)$ = gamma function
$\phi(\chi^2)$ = chi square function

LITERATURE CITED

1. Bennet, C. A., and N. L. Franklin, "Statistical Analysis in Chemistry and Chemical Industry," John Wiley, New York (1954).
2. Pearson, K., "Tables of Incomplete Γ-Functions." Cambridge Univer. Press (Reissue 1946).
3. Winter, O., MS thesis, Univ. Hannover 1960.
4. Davidson, J. F., and D. Harrison "Fluidized Particles," Cambridge Univer. Press (1963).
5. Yasui, G., and L. N. Johanson, *AIChE J.* **4**, 445 (1958).
6. Baumgarten, P. K., and R. L. Pigford, *ibid.*, **6**, 115 (1960).
7. Harrison, D., and L. S. Leung, Paper presented at the Symposium of Interaction between Fluids and Particles, London, England (June 1962).
8. Boettger, G., MS thesis, Univ. Hannover (1957).
9. Heidel, K., *ibid.*, (1959).
10. Shuster, W. W., and P. Kisliak, *Chem. Eng. Prog.*, **48**, 455 (1951).
11. Henwood, G. A., and G. A. Thomas, *Instr. Pract.* 606 (1954).
12. Baerns, M., F. Fetting, and K. Schuegerl, *Chem. Eng. Techn.* **35**, 609 (1963).
13. Winter, O., Ph.D. dissertation, Univ. Hannover (1963).
14. ———, K. Schuegerl, F. Fetting, and G. Schiemann, *Chem. Eng. Sci.* **20**, 823, 839 (1965).

Manuscript received February 24, 1967; revision received August 4, 1967; paper accepted August 9, 1967. Paper presented at AIChE Houston meeting.

Prediction of Drag Reduction with a Viscoelastic Model

G. K. PATTERSON and J. L. ZAKIN

University of Missouri, Rolla, Missouri

VISCOELASTIC THEORIES OF DRAG REDUCTION

A number of polymer solutions which show drag reduction in turbulent flow also exhibit elastic properties in laminar flow. This fact led Dodge and Metzner (*1, 2*) to postulate that the anomalous results they obtained in turbulent-friction-factor measurements in carboxymethyl-cellulose (CMC)–water solutions were caused by elasticity. Savins (*3*) concluded that the elasticity of the polymer solutions studied caused the turbulent fluctuations to be damped and that this damping caused drag reduction. Savins did not propose quantitative expressions to describe the damping postulated.

Some evidence of turbulence damping has been experimentally observed by Shaver and Merrill (*4, 5*) and by Meter (*6*) in dye-injection experiments. Meter recognized the need to correlate drag reduction with elasticity in a quantitative manner. Using a cone-and-plate rheogoniometer and a vibrating rod (0.1 to 400 cycles/sec. Birnboim-Ferry apparatus), Meter measured elastic phenomena in Natrosol (hydroxyethyl cellulose), carboxymethyl-cellulose (CMC), and Carbopol (carboxypolymethylene) solutions. He obtained higher elasticities for Carbopol (non-drag-reducing in turbulent flow) than for CMC at infinitesimal shear rates. This anomaly was attributed to gel formation in the Carbopol solutions.

Meter devised an empirical correlation based on the ratio of wall shear stress to the shear stress $\tau_{1/2}$ at $\mu_o/2$ for his Natrosol-solution friction factor data, where μ_o is the zero shear rate viscosity of the solution. This correlation was recognized by Meter to lack generality because $\tau_{1/2}$ does not exist for dilute solutions, some of which are drag reducing. This correlation may also be criticized in that it implies that elastic phenomena may be correlated as a function of solution viscosity. The elastic phenomena for a given polymer in solution may be a single-valued function of solution viscosity, if elasticity and viscosity are related to concentration in the same way. On this basis Fabula (*7*) was able to relate the drag reduction of a series of polyethylene oxide (Polyox)–water solutions to the intrinsic viscosity, which is a function of molecular size in solution. Correlations of this type, however, have not been shown to be generally applicable to different polymer-solvent systems.

One of the properties of viscoelastic liquids which is frequently measured is the normal stress difference in laminar shear flow. Normal stress differences in laminar flow through a capillary tube are of greatest importance, since capillary-tube flow can yield the high shear rates of interest in turbulent drag reduction. The normal stresses in the axial (P_{xx}), radial (P_{rr}), and tangential ($P_{\theta\theta}$) directions are probably all different in the flow of a viscoelastic fluid. The difference usually measured is ($P_{xx} - P_{rr}$), the first normal stress difference.

Shertzer and Metzner (*8, 9*) measured this normal stress difference for Dow's J-100 and Enjay's Vistanex L-100 (polyisobutylene) solutions by measuring the jet thrust of the polymer solutions issuing from a capillary. The method has a serious shortcoming in that significant normal stress values cannot be measured for dilute polymer solutions (below 0.1%), where a high degree of drag reduction has been observed by several investigators [Hershey and Zakin (*10, 11*), Fabula (*7*), Elata et al. (*12, 13*), Lindgren (*14*), Meyer (*15*), and Ernst (*16*)], because the viscosities of dilute solutions are low, giving high Reynolds numbers (in the turbulent regime) at measurable thrusts. Shertzer (*8*) reported unusual effects in ($P_{xx} - P_{rr}$) measurements above a Reynolds number of 1,000.